# Moiré image patterns on double-walled carbon nanotubes observed by scanning tunneling microscopy

Nobuyuki Fukui,[1] Yuji Suwa,[2] Hiromichi Yoshida,[1] Toshiki Sugai,[1] Seiji Heike,[2] Masaaki Fujimori,[2] Yasuhiko Terada,[3] Tomihiro Hashizume,[2,4,5] and Hisanori Shinohara[1,*]

[1]*Department of Chemistry and Institute for Advanced Research, Nagoya University, Nagoya 464-8602, Japan*

[2]*Advanced Research Laboratory, Hitachi, Ltd., Hatoyama, Saitama 350-0395, Japan*

[3]*Institute of Applied Physics, University of Tsukuba, Tsukuba, Ibaraki 305-8573, Japan*

[4]*Department of Physics, Tokyo Institute of Technology, Meguro, Tokyo 152-8551, Japan*

[5]*WPI Advanced Institute for Materials Research, Tohoku University, Sendai 980-8577, Japan*

(Received 28 June 2008; revised manuscript received 23 December 2008; published 4 March 2009)

Long-range quasiperiodic patterns are found in scanning tunneling microscopy (STM) images of double-walled carbon nanotubes (DWNTs) on top of the atomic images of six-membered carbon rings of the outer tubes. By comparing the results of first-principles calculations on model DWNTs, we conclude that they are moiré patterns showing local modulations of electronic states due to the interlayer interactions between the outer and inner tubes. We also demonstrate that these moiré patterns can be used to assign the chiral vector of the inner tube of a DWNT which is usually inaccessible by STM.

DOI: 10.1103/PhysRevB.79.125402 PACS number(s): 73.63.Fg, 61.48.De, 68.37.Ef

## I. INTRODUCTION

Recent developments in the synthesis and purification methods of carbon nanotubes (CNTs) (Ref. 1) have enabled us to prepare high-quality double-walled carbon nanotubes (DWNTs) (Ref. 2) with few defects. The DWNTs have aroused great scientific interest as they can be compared with bilayer graphene sheets having unusual quantum properties.[3,4] The typical diameter of DWNTs is slightly larger than that of single-walled carbon nanotubes (SWNTs) with a certain interlayer distance.[5] Atomic images of SWNTs have been observed by scanning tunneling microscopy (STM), and a unique relationship between their electronic properties and geometries was reported.[6–8] Various types of CNTs such as fullerene- or metallofullerene-encapsulated SWNTs[9,10] (so-called nanopeapods) were also observed by STM.

Electronic structures of SWNTs are categorized as semiconductive and pseudometallic depending on their chirality. The band-gap energies of semiconductive SWNTs are inversely proportional to diameters;[11] thereby, multiwalled carbon nanotubes (MWNTs) with large diameters are nearly metallic. To investigate these characteristics of CNTs, STM is one of the most powerful tools, which enables us to measure the electronic local density of states near the Fermi level with an atomic resolution. In fact, moiré patterns due to the modulations of the electronic states are obtained by STM[12,13] when graphite surfaces are modified by defects or domain boundaries. Very recently, STM images of DWNTs have been reported,[14] which are almost the same as atomic images of SWNTs.

In this paper, we show STM images of DWNTs obtained at certain bias voltages, exhibiting long-range quasiperiodicities, i.e., moiré patterns, on top of atomic images of six-membered carbon rings of the outer tubes. First-principles calculations on model DWNTs show that these moiré patterns can be understood as the result of interactions between the inner and outer tubes of DWNTs. We can assign possible candidates for chiral vectors of the inner and outer tubes from these images and simulations. This kind of interlayer interaction in DWNTs will be of great importance for discussing electron transport properties in devices made of DWNTs such as high-performance DWNT field-effect transistors.[15]

## II. EXPERIMENTAL

The DWNTs used in this work were synthesized using the pulse-arc discharge method enriched by thermal oxidation.[2] Composite graphite rods with ytterbium and nickel (4.5 and 1.5 at. %, respectively) were first vaporized in an Ar atmosphere by pulsed-arc discharge while maintaining the temperature of the arc discharge area at 1323 K by an electric furnace. Then, the CNT sample was purified by thermal oxidation at 673 K for 90 min in the electric furnace, and the by-product SWNTs were partially removed. The CNT sample was further treated with concentrated hydrochloric acid to remove the catalyst and was rinsed with sodium hydrogen carbonate and distilled water. After the sample was dried in air, the dilute DWNT solutions were prepared by dispersing them into chloroform with ultrasonication.

The Cu(111) surface was prepared by repeated annealing and Ar sputtering processes in ultrahigh vacuum (UHV). The DWNTs were cast onto the Cu(111) substrate by using pulsed-jet deposition[16] at $10^{-6}$ Pa at 323 K. The shutter opening time per pulse was set to 2 ms, and the corresponding amount of the CNT solution injected per pulse was typically 2 $\mu l$. The pulsed-jet deposition was performed with 100 pulses in total. The substrate was cleaned from time to time by heating at 780 K in UHV to prevent contamination of the Cu surface. After the injection, the Cu(111) substrate was heated at 780 K for 10 min in UHV. The W tips were prepared by chemical etching and by checking the field ion

 

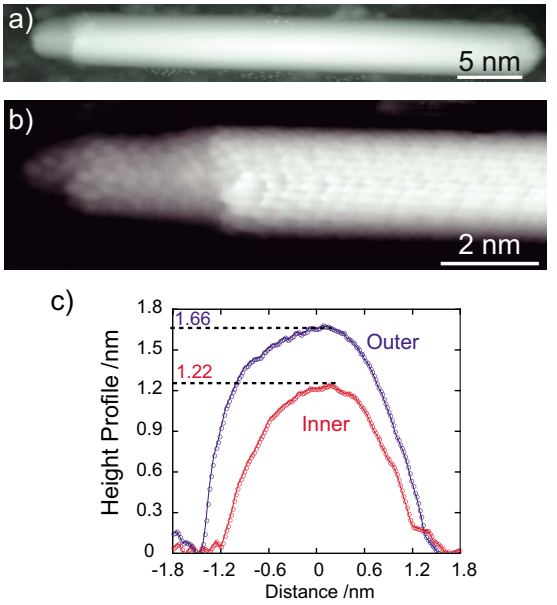


FIG. 1. (Color online) (a) STM image of a DWNT ($V_{sample}$ =−2.0 V and $I_{tunnel}$=10 pA). The left part (~4 nm) has a different apparent height and is assigned as the peeled-off inner tube of the DWNT. (b) Magnified image of (a) with a bias voltage tuned for observing density of states modulation ($V_{sample}$=−0.3 V and $I_{tunnel}$ =20 pA). Near the left end of the outer tube and on the inner tube, the interference patterns of the local density of states emerge. The interference pattern on the outer tube extends approximately 2 nm from the edge of the outer tube and is gradually suppressed. (c) Cross-sectional views of height profiles measured for the inner and outer tubes in (b).

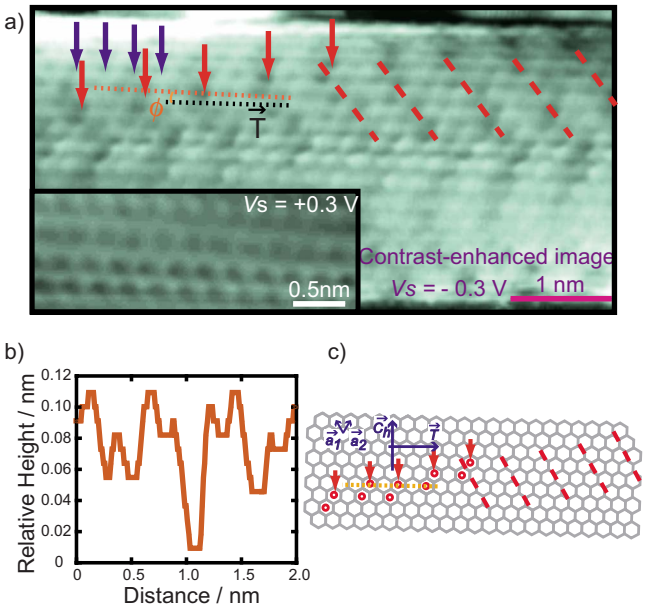


FIG. 2. (Color online) Superstructures of the DWNT observed with a low-bias STM image. (a) Magnified STM image of the right part of the DWNT in Fig. 1(b) with enhanced contrast ($V_{sample}$ =−0.3 V). A long-range quasiperiodic pattern is observed. The atomic corrugation corresponds to six-membered carbon rings (dark blue arrows). The long-range periodicity (red arrows and red dashed lines) is approximated by (−2,3) using $a_1$ and $a_2$ unit vectors shown in (c). The wrapping angle ($\phi$) corresponds to the angle between the armchair direction (dotted orange line) and the tube axis (dotted black line). The inset shows a STM image using a different bias voltage ($V_{sample}$=+0.3 V), where the long-range periodicity cannot be observed. (b) Cross-sectional line profile of dotted orange line in (a). (c) Schematic expression of the moiré patterns with long-range periodicity. The red circles indicate darkly observed six-membered carbon rings in (a).

microscope images in the UHV chamber to shape the tip apex.[17] All the STM measurements were performed in a homemade UHV-STM at room temperature.

## III. RESULTS AND DISCUSSION

### A. STM image of DWNTs

Figure 1(a) shows a STM image of a DWNT ($V_{sample}$ =−2.0 V and $I_{tunnel}$=10 pA) on a Cu(111) surface. As can be clearly seen, the diameter of the left edge, where the end of the outer tube has been peeled off, is smaller than the rest of the nanotube. Figure 1(b) shows a low-bias STM image of the left end part of the DWNT in Fig. 1(a) ($V_{sample}$ =−0.3 V and $I_{tunnel}$=20 pA). The apparent heights of the inner and outer tubes are approximately 1.22 and 1.66 nm (±0.05 nm), respectively, which correspond to the interlayer distance of approximately 0.4 nm [cf. Fig. 1(c)]. These apparent heights of inner and outer tubes of DWNTs vary up to approximately 0.5 nm depending on the bias voltage and tunneling current.[7,18] The interlayer distance of the DWNTs $d_{io}$ estimated from the STM image agrees well with the reported range (0.35–0.45 nm) measured by high-resolution transmission electron microscopy (TEM).[5] Furthermore, electron-scattering patterns can be observed with atomic defects in Fig. 1(b). These patterns on the outer tube extend approximately 2 nm from the end of the outer tube, which is consistent with a previous report.[6]

Figure 2(a) shows a close-up image of the right part of the DWNT in Fig. 1(b) with enhanced contrast. In this region, the interference pattern due to the end of the tube and/or the defects discussed above is smeared out, but another type of long-range quasiperiodic pattern is observed. Moreover, this pattern was dependent on the scan bias voltage. The wrapping angle of the armchair direction to the tube axis direction of this outer tube ($\phi$)[7] is measured as 2±1° from Fig. 2(a). Similar kinds of electronic modulations for a graphite surface[13] and overlayer growth on a graphite surface[19] have been observed by STM and are theoretically understood to be moirélike modulations in the electronic densities of states due to the interlayer interactions.[20] The long-range periodicity observed in the present DWNT can also be considered as a similar type of moiré pattern due to the interaction between the outer and inner tubes.

The obtained patterns have few relations to the charge transfer (CT) because the position of STM observation is at the top side of the DWNT, away from the back side that is in contact with the substrate. The CT perturbations are localized at the area close to the substrate and are much weaker at the furthest carbon[21] where STM measurements were performed. Also, taking the difference in work function between Cu and Au into account, the work function of Cu is similar to that of

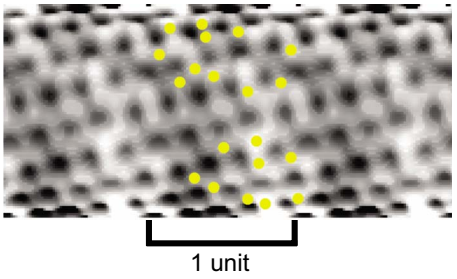


FIG. 3. (Color online) Simulated STM image (gray scale) of the (8,−4)@(12,6) DWNT by first-principles calculations. (The minus number here means that the tube is placed with the opposite direction of helicity.) Brighter and darker regions correspond to the areas with larger and smaller densities of states, respectively. The density of states modulation is analyzed based on the distance between a carbon atom of the inner tube and a carbon atom of the outer tube. The yellow filled circles indicate the distribution of carbon atom pairs with longer atomic distance (distant carbon pairs), which reproduce the brighter area with a larger density of states.

a CNT, and the amount of CT to the CNT from Cu is smaller than that from Au; therefore, we can ignore the effects of CT.

### B. Origin of moiré patterns

The origin of the moiré patterns can be explained as follows: when a carbon atom of the inner tube is located close to a carbon atom of the outer tube (for example, when the inner carbon atom is located directly below the outer carbon atom), the overlap between the $\pi$ orbitals of those atoms becomes large. This can be contrasted with the case when those two atoms are apart, for example, when the carbon atom of the inner tube is located directly below the center of the six-membered carbon ring of the outer tube. We hereafter call these interlayer pairs of carbon atoms "vicinal carbon pairs" and "distant carbon pairs," respectively. Spatial distribution of such interlayer carbon pairs depends on the combination of chiral vectors of the outer and inner tubes.

Because the overlap of the $\pi$ orbitals enlarges the local band gap by forming bonding and antibonding states, energy levels of the electronic states whose wave functions have large amplitudes at vicinal carbon pairs are shifted significantly due to this gap widening effect. On the other hand, energy levels of the states with small amplitudes at those pairs are not shifted substantially. As a result, there should be a certain bias voltage near the band edge where STM fails to pick up the electronic density of states whose energy levels are affected by the overlap while it picks up the unaffected states. At that particular bias voltage, STM obtains spatially uneven images reflecting the distribution of vicinal and distant carbon pairs, i.e., moiré patterns. When the bias voltage is increased, all those electronic states are picked up and spatial unevenness is canceled.

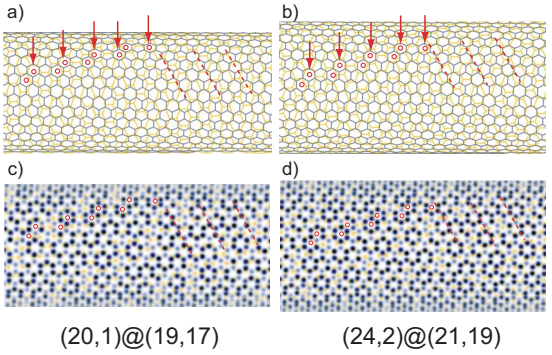


FIG. 4. (Color online) Simulated moiré patterns for possible candidates of DWNTs. (a),(b) Atomic alignment of six-membered carbon rings of inner tubes (yellow lines) and outer tubes (gray lines) for the possible candidates of chiral vectors of DWNTs, (20,1)@(19,17) and (24,2)@(21,19) [(inner-tube chirality)@(outer tube chirality)]. Here, the diameters of the inner tubes are enlarged to fit those of the outer tubes in order to show the inner-tube structure directly below the outer tube *along the radial direction.* (c), (d) Distribution of vicinal carbon pairs for DWNTs in Figs. 4(a) and 4(b). The gray circles show the positions of carbon atoms of the outer tube, and the dark circles indicate the vicinal carbon pairs. The yellow dots show the location, i.e., the projective point, of the carbon atoms of the inner tube, which correspond to the distant carbon pairs. Red arrows, dashed lines, and circles in (a) through (d) show the moiré patterns comparable to those in Fig. 2(a).

TABLE I. Basic parameters of possible candidates of chiralities for DWNT (Fig. 4).

| | Outer | | Inner | | | |
|---|---|---|---|---|---|---|
| | Diameter $d_o$ (nm) | Chiral angle $\theta_o$ (deg) | Diameter $d_i$ (nm) | Chiral angle $\theta_i$ (deg) | Interlayer distance[a] $d_{\text{inter}}$ (nm) | Misorientation angle (deg) |
| (20,1)@(19,17) | 2.443 | 28.16 | 1.607 | 2.42 | 0.418 | 25.74 |
| (24,2)@(21,19) | 2.714 | 28.34 | 1.962 | 2.42 | 0.376 | 25.92 |
| | Apparent height[b] (nm) | Chiral angle $\theta_o$ (deg) | Apparent height[b] (nm) | Chiral angle $\theta_i$ (deg) | Interlayer distance[a] $d_{\text{inter}}$ (nm) | Misorientation angle (deg) |
| Experimental | $1.66 \pm 0.05$ | $28.0 \pm 1.0$ [c] | $1.22 \pm 0.05$ | - | $0.44 \pm 0.1$ | $24.60 \pm 1.43$ |

[a]Interlayer distance is calculated by $d_{\text{inter}}=(d_o-d_i)/2$, DWNTs have coaxial structures.
[b]Experimental apparent heights are modified by the substrate ($V_{\text{sample}}=-0.3$ V and $I_{\text{tunnel}}=20$ pA; refer to Sec. III D).
[c]Chiral angle of outer tube is calculated by $\theta_o=30-\phi$, where $\phi$ is the wrapping angle with tube axis.

### C. First-principles calculation

In order to see how the interlayer interaction affects STM images, we have performed first-principles calculations of several DWNTs with small chiral vectors, such as $(8,-4)@(12,6)$, $(4,2)@(10,5)$, $(8,4)@(14,7)$, etc. Although they are smaller than that of the observed DWNTs, they are scarce calculable examples of DWNTs without edges of the graphene sheet owing to periodic boundary conditions. In most cases, a pair of CNTs with arbitrary chiral indexes has no common multiple of the unit lattice lengths along the tube axis, i.e., most DWNTs are incommensurate. Among a few exceptional commensurate DWNTs, we had to choose one whose unit lattice length and diameters were small enough for first-principles calculation (about 300 carbon atoms in the unit cell at most). We avoided treating models of DWNTs with edges of the graphene sheet because they would have strongly affected the STM images.

Figure 3 shows a simulated STM image ($V_{\text{sample}}=-0.5$ V) of a DWNT with $(8,-4)@(12,6)$ chirality. Electronic states are calculated using generalized gradient approximation[22] with ultrasoft pseudopotentials.[23,24] The energy cutoff of the plane wave basis is taken to be 20.25 Ry. Figure 3 is created according to the height of the isosurface of the STM current density.[25] Here, the height due to a cylindrical shape of the nanotube is compensated in order to enhance surface patterns. The same correction was also applied to the experimental STM images such as in Fig. 2(a).

Here, it should be noted that the DWNT used for calculating Fig. 3 has an interlayer distance of 0.21 nm, which is small compared to the typical values for DWNTs. We did not find moiré patterns in the simulation for the DWNTs with $d_{io}=0.32$ nm [such as $(4,2)@(10,5)$ and $(8,4)@(14,7)$] and 0.42 nm [such as $(6,3)@(14,7)$]. There are no calculable models of DWNTs with an interlayer distance between 0.21 and 0.32 nm. The reason we have not found moiré patterns in the DWNTs with $d_{io}>=0.32$ nm is the limit of the calculation accuracy. Because the moiré pattern comes from the small fluctuations of the electronic states, highly accurate calculation is required to reproduce it. The interlayer interaction for $d_{io}=0.32$ nm is so small that the present calculation could not achieve the necessary accuracy, and thus the small modulation of the electronic states is lost in noise. Because the interlayer interaction is large enough in DWNTs with $d_{io}=0.21$ nm, we can simulate the moiré patterns. By this calculation, we illustrated that the spatial fluctuation of interlayer interaction due to uneven distribution of vicinal carbon pairs can cause moiré patterns. Although the interlayer interaction of the present model is very large, the electronic states of each tube do not essentially change. We do not discuss here whether the interlayer interaction of the observed DWNTs is strong enough to make moiré patterns that are detectable in the STM experiment.

It should also be noted here that the moiré pattern in Fig. 3 is obtained for the structure without geometry optimization. When the geometry optimization is performed, either the outer or inner tube is shifted by a few tenths of nanometers along the tube axis. We could not find a moiré pattern after that. This fact indicates two things. One is that the existence of crowded regions and empty regions with vicinal or distant carbon pairs is important. In Fig. 3, the yellow filled circles indicate distribution of distant carbon pairs. Due to the shift of the nanotube, the distribution of such regions changed, and the moiré pattern disappeared. The second is that the structure causing the moiré pattern is not energetically favorable. This fact does not necessarily mean that DWNTs exhibiting moiré patterns rarely exist. Because the DWNTs we have calculated are commensurate and their unit lattice lengths are small, they can relax by a relative shift of the inner or outer tube along the tube axis. On the other hand, most existing DWNTs are incommensurate, and thus they cannot relax by such a shift, i.e., even though the electronic energy due to the interlayer interaction is lowered by a shift at some regions, it is always raised at some other regions. Therefore, the moiré pattern we found in our experiment is not a rare example. Many existing DWNTs are expected to have such patterns.

### D. Assignment of DWNTs

Next, we discuss periodicity of the moiré pattern observed in Fig. 2(a). Based on a previous report of the graphite case, the periodicity of the moiré pattern $D$ is expressed as $D=d/[2\sin(\theta/2)]$, where $d$ and $\theta$ represent the lattice constant of graphene sheets and the misorientation angle of the two graphene sheets,[26] respectively. In the case of graphite, the moiré pattern shows isotropic threefold symmetry. For the DWNTs, the interaction between carbon atoms of the inner and outer tubes needs to be considered, particularly along the radial direction. The unit distance of six-membered carbon rings is, however, common to both tubes along the circular direction, and thus there always exists a gradual mismatch between the positions of carbon atoms in the inner and outer tubes. There is no such gradual mismatch along the axial direction because the two layers are parallel along that direction.

We are now able to choose the probable candidates for chiral vectors of the inner and outer tubes of a DWNT. The candidates for the outer tube are selected from nanotubes that have diameters larger than 1.66 nm and have wrapping angles within the range of $2\pm1°$. To narrow down the candidates, we used the fact that the number of visible six-membered rings arranged in the width direction of the outer tube in Fig. 2(a) is about 16. This fact roughly limits the diameters within the range of $2.6\pm0.3$ nm. Although this is fairly larger than that estimated from the apparent height (1.66 nm), it is not surprising because apparent heights of CNTs are known to be underestimated frequently due to the difference between the tip-sample interaction and tip-substrate interaction.[7,8] The candidates for the inner tube are selected so that the interlayer distance is approximately 0.4 nm. The difference of the apparent height between the outer tube and inner tube (0.4 nm) is reliable because of the same tip-sample interactions. Finally, the combinations of inner and outer tubes are considered taking account of the moiré pattern. The most probable candidates for the DWNT in Fig. 2(a) are $(20,1)@(19,17)$ or $(24,2)@(21,19)$. The structural models and parameters of the two candidates are shown in Fig. 4 and Table I, respectively.

The DWNTs in the present work and previous reports[5,14] have larger interlayer distances (~0.4 nm or more) than that of graphite (0.34 nm) and those of typical MWNTs. This suggests that electronic interactions in DWNTs by the curvature effects of $\pi$ electrons[27] are also important. A long-range modulation of electronic local density of states in a MWNT was also reported.[28] This can be understood if we recall that the long-range wave functions of electrons have longer decay length and propagate through multigraphene layers.[20]

## IV. CONCLUSION

In summary, we have observed bias-dependent STM images of DWNTs. The DWNTs show two periodic structures: an ordinary pattern formed by six-membered carbon rings and a moiré pattern with long-range periodicity that is induced by the interlayer interaction between the outer and inner tubes of DWNTs. Analysis using first-principles calculations has revealed that the modulation of the electronic local density of states can be explained by the distribution of vicinal and distant carbon pairs. The present technique using STM observations can be widely used to obtain chiral vectors of outer and inner tubes of DWNTs.

## ACKNOWLEDGMENTS

Thanks are due to the CREST Program on Novel Carbon Nanotube Materials by JST and to the Special Coordination Funds for Promoting Science and Technology of the MEXT.

*noris@cc.nagoya-u.ac.jp

[1] S. Iijima, Nature (London) **354**, 56 (1991).
[2] T. Sugai, H. Yoshida, T. Shimada, T. Okazaki, H. Shinohara, and S. Bandow, Nano Lett. **3**, 769 (2003).
[3] G. M. Rutter, J. N. Crain, N. P. Guisinger, T. Li, P. N. First, and J. A. Stroscio, Science **317**, 219 (2007).
[4] R. V. Gorbachev, F. V. Tikhonenko, A. S. Mayorov, D. W. Horsell, and A. K. Savchenko, Phys. Rev. Lett. **98**, 176805 (2007).
[5] A. Hashimoto, K. Suenaga, K. Urita, T. Shimada, T. Sugai, S. Bandow, H. Shinohara, and S. Iijima, Phys. Rev. Lett. **94**, 045504 (2005).
[6] H. Kim, J. Lee, S. J. Kahng, Y. W. Son, S. B. Lee, C. K. Lee, J. Ihm, and Y. Kuk, Phys. Rev. Lett. **90**, 216107 (2003).
[7] J. W. G. Wildör, L. C. Venema, A. G. Rinzler, R. E. Smalley, and C. Dekker, Nature (London) **391**, 59 (1998).
[8] T. W. Odom, J.-L. Huang, P. Kim, and C. M. Lieber, Nature (London) **391**, 62 (1998).
[9] D. J. Hornbaker, S. J. Kahng, S. Misra, B. W. Smith, A. T. Johnson, E. J. Mele, D. E. Luzzi, and A. Yazdani, Science **295**, 828 (2002).
[10] J. Lee, H. Kim, S. J. Kahng, G. Kim, Y. W. Son, J. Ihm, H. Kato, Z. W. Wang, T. Okazaki, H. Shinohara, and Y. Kuk, Nature (London) **415**, 1005 (2002).
[11] R. Saito, G. Dresselhaus, and M. S. Dresselhaus, J. Appl. Phys. **73**, 494 (1993).
[12] H.-L. Sun, Q.-T. Shen, J.-F. Jia, Q.-Z. Zhang, and Q.-K. Xue, Surf. Sci. **542**, 94 (2003).
[13] H. A. Mizes and J. S. Foster, Science **244**, 559 (1989).
[14] C. E. Giusca, Y. Tison, V. Stolojan, E. Borowiak-Palen, and S. R. P. Silva, Nano Lett. **7**, 1232 (2007).
[15] T. Shimada, T. Sugai, Y. Ohno, S. Kishimoto, T. Mizutani, H. Yoshida, T. Okazaki, and H. Shinohara, Appl. Phys. Lett. **84**, 2412 (2004).
[16] N. Fukui, A. Taninaka, T. Sugai, H. Yoshida, S. Heike, M. Fujimori, Y. Terada, T. Hashizume, and H. Shinohara, J. Nanosci. Nanotechnol. **7**, 4267 (2007).
[17] T. Hashizume, K. Motai, X. D. Wang, H. Shinohara, Y. Saito, Y. Maruyama, K. Ohno, Y. Kawazoe, Y. Nishina, H. W. Pickering, Y. Kuk, and T. Sakurai, Phys. Rev. Lett. **71**, 2959 (1993).
[18] L. Tapasztó, G. I. Márk, A. A. Koós, P. Lambin, and L. P. Biró, J. Phys.: Condens. Matter **18**, 5793 (2006).
[19] B. A. Parkinson, F. S. Ohuchi, K. Ueno, and A. Koma, Appl. Phys. Lett. **58**, 472 (1991).
[20] K. Kobayashi, Phys. Rev. B **53**, 11091 (1996).
[21] Y. Xue and S. Datta, Phys. Rev. Lett. **83**, 4844 (1999).
[22] J. P. Perdew, K. Burke, and Y. Wang, Phys. Rev. B **54**, 16533 (1996).
[23] D. Vanderbilt, Phys. Rev. B **41**, 7892 (1990).
[24] K. Laasonen, A. Pasquarello, R. Car, C. Lee, and D. Vanderbilt, Phys. Rev. B **47**, 10142 (1993).
[25] J. Tersoff and D. R. Hamann, Phys. Rev. Lett. **50**, 1998 (1983).
[26] M. Kuwabara, D. R. Clarke, and D. A. Smith, Appl. Phys. Lett. **56**, 2396 (1990).
[27] T. Kawase and H. Kurata, Chem. Rev. (Washington, D.C.) **106**, 5250 (2006).
[28] M. Ge and K. Sattler, Science **260**, 515 (1993).